SANDIA REPORT
SAND2019-12390
Printed Click to enter a date

Sandia National Laboratories

Microstructural Modification and Healing of Additively Manufactured Parts by Electropulsing

Philip J. Noell, Jeffrey M. Rodelas, Zahra Ghanbari, Christopher M. Laursen

Prepared by
Sandia National Laboratories
Albuquerque, New Mexico
87185 and Livermore,
California 94550

Issued by Sandia National Laboratories, operated for the United States Department of Energy by National Technology & Engineering Solutions of Sandia, LLC.

Available to DOE and DOE contractors from
U.S. Department of Energy
Office of Scientific and Technical Information
P.O. Box 62
Oak Ridge, TN 37831

Telephone: (865) 576-8401
Facsimile: (865) 576-5728
E-Mail: reports@osti.gov
Online ordering: http://www.osti.gov/scitech

Available to the public from
U.S. Department of Commerce
National Technical Information Service
5301 Shawnee Rd
Alexandria, VA 22312

Telephone: (800) 553-6847
Facsimile: (703) 605-6900
E-Mail: orders@ntis.gov
Online order: https://classic.ntis.gov/help/order-methods/

ABSTRACT

For many applications, the promises of additive manufacturing (AM) of rapid development cycles and fabrication of ready-to-use, geometrically-complex parts cannot be realized because of cumbersome thermal postprocessing. This postprocessing is necessary when the non-equilibrium microstructures produced by AM lead to poor material properties. This study investigated if electropulsing, the process of sending high-current-density electrical pulses through a metallic part, could be used to modify the material properties of AM parts. This process has been used to modify conventional wrought materials but has never been applied to AM materials. Two representative AM materials were examined: 316L stainless steel and AlSi10Mg. Two hours of annealing are needed to remove chemical microsegregation in AM 316L; using electropulsing, this was accomplished in 200 seconds. The ductility of AlSi10Mg parts was increased above that of the as-built material using electropulsing. This study demonstrated that electropulsing can be used to modify the microstructures of AM metals.

ACKNOWLEDGEMENTS

The authors would like to acknowledge Jay Carroll for beneficial discussions and supplying material. Also, the authors would like to acknowledge Zachary Casias, Peter Duran, John Laing, Sara Dickens, Celedonio Jaramillo, Renae Hickman, and Christina Profazi for their exceptional experimental support.

Contents

ACRONYMS AND DEFINITIONS

Abbreviation	Definition
AM	Additively Manufactured
AlSi10Mg	Aluminum Silicon Magnesium
SS	Stainless Steel
SLM	Selective Laser Melting
TD	Tensile direction
LTD	Long transverse direction
STD	Short transverse direction
EBSD	Electron backscatter diffraction
IPF	Inverse pole figure
KAM	Kernel average misorientation
HV	Vickers hardness
EDS	Energy dispersive X-ray microscopy

1. MICROSTRUCTURAL MODIFICATION OF ADDITIVELY MANUFACTURED PARTS BY ELECTROPULSING

1.1. Introduction

Additive manufacturing (AM) is a rapid, flexible technique for manufacturing complex metallic components. Selective laser melting (SLM), also called laser powder bed fusion or direct metal laser sintering, is an AM technique which uses a laser to selectively melt a bed of metal powder. Each layer of melted metal is deposited on the previous layer, allowing the fabrication of near-net-shape parts. Because the melted material in each layer is rapidly cooled by the surrounding powder, as-built SLM parts are far from equilibrium. Microstructural features such as non-equiaxed grains, strong textures, significant residual density of dislocations, and chemical segregation are thus typical of as-built SLM parts. These features can lead to high hardness and strength but are also often associated with lowered ductility and corrosion resistance compared to conventional wrought materials [1-5]. At present, post-build heat treatments are commonly employed to decrease chemical microsegregation, reduce residual stresses, and/or produce equiaxed grains with random textures [2, 4]. There are, of course, significant downsides to adding an additional processing step to SLM parts such as decreased part throughput and increased lead time. Heat treatment is occasionally unfeasible due to part warpage during high-temperature exposure. Moreover, a recent study of 304L stainless steel fabricated by directed energy deposition, an AM technique that produces microstructures similar to SLM, demonstrated that significantly higher temperatures and longer exposure times were necessary to remove chemical microsegregation and cause recrystallization than in a comparable wrought material [6]. Similar observations have been reported for SLM 316L [7]. The present study thus examines an alternative method for postprocessing SLM, and by extension all metallic AM materials: electropulsing.

Electropulsing is defined as the passage of electrical current through a material [8]. This can be done both by application of a continuous current and multiple high-current density pulses of short duration, typically in the form of controlled electrical pulses. Since the pioneering work of Troitskii in the 1960's [9-10], this technique has been applied to many materials, including copper [11], steels [12-13], and aluminum alloys [14-15]. Many effects have been observed, including:

1. accelerated recrystallization [11, 14, 16-17],
2. crystallization of amorphous alloys [18-19],
3. crack closure [16], and
4. accelerated phase transformations [20-21]

Historically, most studies of electropulsing focused on the capacity of electropulsing to produce recrystallization much more rapidly and with significantly less heat input that traditional heat treating [11, 14, 16-17]. Similarly, studies of amorphous materials demonstrated that electropulsing can lead to partial or complete crystallization of the microstructure, depending on the current density and number of pulses alloys [18-19]. Electropulsing has also been observed to partially or completely close cracks and pores in materials, particularly at relatively low current densities ($I \approx 10^{-1}$ kA/mm^2) [22]. More recently, several studies have demonstrated that electropulsing can influence the precipitation and aging of second-phase particles and intermetallic compounds. In their study of a

Cu-Zn alloy with lead inclusions, Wang *et al.* observed that electropulsing formed many, small lead particles segregated to grain boundaries rather than the few, large lead particles consistently observed following various heat treatments [23]. Electropulsing of pearlitic steels has been observed to lead to fragmentation of the lamellar structure the formation of nanoscale γ-Fe particles [24-25]. In stainless steels, Qin and coworkers observed that electropulsing 316 stainless steel (SS) during annealing reduced the average size of χ-phase particles by a factor of 5 [26].

However, compared to conventional diffusion-controlled heat treatment processes, there is little understanding of the mechanisms that control microstructural evolution during electropulsing. Broadly speaking, three mechanism have been proposed: Joule heating, electron wind, and altering the activation energy [8, 13, 15, 20]. Joule heating is the process by which passing an electric current through a conductor produces heat. While Joule heating may play a role in electropulsing at all current densities, it appears to dominate at current densities below $\approx 10^0$ kA/mm^2 [27-29]. At current densities greater than $\approx 10^0$ kA/mm^2, the effects of electropulsing cannot be explained by Joule heating alone [8, 13]. It is thus thought that electropulsing induces changes in the microstructure by some combination of electron wind effects and by altering the activation energy of the material. The term electron wind refers to the force caused by the exchange of momentum between ionized atoms and other charge carriers in a material when current is passed [30-31]. This phenomenon has long been studied in the field of electromigration [31]. The importance of electron wind to electropulsing is, however, unclear. It is commonly used to explain electropulsing-induced recrystallization because the electron wind force may be capable of enhancing the mobility of dislocations [21, 32-33]. It is also thought that the additional free energy associated with applying an electric current, ΔG^e, plays a key role in electropulsing at currents greater than $\approx 10^0$ kA/mm^2 [8, 13]. Decoupling the effects of these various mechanisms remains challenging, though. Because of this, the combination of electrical current density, pulse duration, and exposure time are empirically determined for each material. Moreover, it is usually unknown *a priori* what microstructural changes to expect when a given material is subjected to electropulsing [34]. Prior studies have primarily examined wrought sheet materials, and desirable microstructural changes were only attained in some cases. Moreover, compared to conventional wrought or cast materials, SLM materials are far from equilibrium and contain complex non-equilibrium chemical and dislocation substructures as well as complex non-equilibrium grain structures. It is thus unclear if and how electropulsing will affect the microstructure and properties of materials manufactured by SLM as such studies have never been conducted.

This study examines if electropulsing can be used to alter chemical segregation in additively manufactured materials. Two alloy systems were selected for this study: 316L stainless steel (316L SS) and AlSi10Mg. These material systems were chosen both because of their widespread use and because of the significantly different microstructures produced when these materials are processed by SLM. 316L SS is an austenitic stainless steel that offers improved corrosion resistance relative to 304L, moderate strength via solid solution strengthening, and excellent ductility. The rapid solidification behavior of 316L under non-equilibrium conditions such as metal additive manufacturing is largely similar to high-energy density welding as reported in detail in the technical literature [35-36]. Like 304L, the solidification microstructure of AM 316L depends largely on the starting alloy composition; however, most 316L alloy compositions subject to SLM solidify as austenite with no terminal solidification products [37-39]. The solidification substructure exhibits

elemental partitioning of principally ferrite-promoting alloying elements such as chromium, molybdenum, and silicon [40]. This microsegregation can lower the corrosion resistance of the material, as discussed by Trelewicz *et al* [1]. While austenitic stainless steel solidification microstructures are not typically heat treated after fabrication there have been a number of studies in the technical literature that show solutionizing annealing heat treatment can eliminate microsegregation, dislocation networks, and/or or promote recrystallization in microstructures produced via AM [6-7].

AlSi10Mg is a hypoeutectic aluminum-silicon-magnesium alloy that is an appealing candidate for SLC due to its light weight and low melting point [4, 41]. Another considerable advantage to AlSi10Mg is that it is a casting alloy with intrinsically good solidification behavior. As-fabricated AlSi10Mg materials typically exhibit a cellular/cellular-dendritic solidification substructure containing primary α-Al dendrites surrounded by α-Al + silicon terminal interdendritic eutectic constituent [2, 4]. After fabrication, this material is typically heat treated at 300° C for 120 minutes, which results in eutectic Si particle coarsening and precipitation of Si in the primary α-Al phase [2, 4]. This heat treatment also significantly changes the mechanical properties of the material, decreasing the ultimate tensile strength (UTS) from approximately 380 MPa to 250 MPa and increasing the ductility from approximately 2% to 10 to 18% [3]. While less common, other heat treatment methods have been examined, including the T6 heat-treatment typically used for 6000-series Al alloys. This heat treatment involves a solution heat treatment for 1 hour at 520° C followed by artificial ageing for approximately 6 hours at 160° C [42]. The mechanical properties of AlSi10Mg materials after several different heat treatment methods are summarized in Table 1-1. The general effect of all these heat treatments is to alter the distribution of the Si-rich phase, as discussed in references [2, 5].

Table 1-1. For the studies referenced, this table summarizes the ultimate tensile stress (UTS), total elongation, and Vickers hardness of AlSi10Mg materials after various heat treatments (HT). For comparison, the as-fabricated (AF) properties of the material used in the study are listed in parentheses after each value.

Heat-treatment	Vickers hardness	Ultimate tensile strength (MPa)	Elongation (%)	Reference
300° C, 2 hours	-	285 (475)	18.6 (7.5)	[2]
530° C, 6 hours	-	269 (475)	18.3 (7.5)	[2]
240° C, 0.25 hours	124 (128)	-	-	[5]
282° C, 0.25 hours	108 (128)	-	-	[5]
307° C, 0.25 hours	98 (128)	-	-	[5]
450° C, 0.50 hours	58 (128)	-	-	[5]
T6	-	300 (350)	2.5 (3)	[43]
T6	-	280 (320)	4.5 (1.25)	[42]

In the present study, SLM 316 SS and AlSi10Mg materials were electropulsed using a Gleeble® 3800 using alternating current (AC) current (60 Hz) under atmospheric conditions. Direct current (DC) is typically used for electropulsing, but a previous study demonstrated that electropulsing can also be

performed using AC [28]. AC was chosen for this study due to the availability of the Gleeble® to perform electropulsing; future work will be done to examine the effect of using DC to electropulse SLM materials. The focus of this work was to understand of electropulsing could be used to (1) control chemical microsegregation in SLM 316 SS and (2) the distribution of second-phase particles in AlSi10Mg.

1.2. Materials and Methods

Two factors were considered when designing specimens. First, it was desirable to be able to grip specimens using the Gleeble®® 3500 (Dynamic Systems Inc., Poestenkill, NY) thermo-physical simulator (described in a subsequent paragraph). Second, it was desirable to be able to perform tensile tests on samples after electropulsing. Because of this, tensile dogbones, such as the one shown in Figure 1, were utilized in this study. The specimens were of a uniform thickness of 2.5 mm. The gauge width was 2.5 mm and the gauge length was 10 mm, with a 45° fillet between the grip and gauge regions.

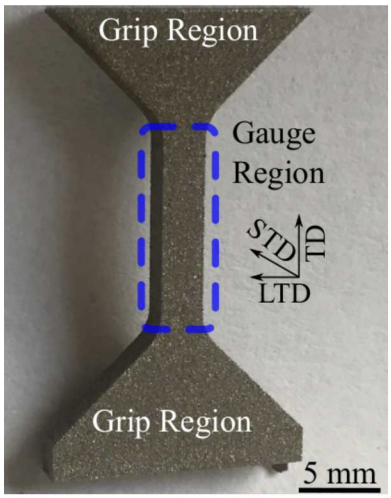

Figure 1. ***An optical image of a stainless steel tensile specimen used in this study is shown. The gauge and grip regions are labelled. The primary specimen directions are labelled as follows: tensile direction (TD), long transverse direction (LTD), and short transverse direction (STD).***

316L SS samples were manufactured using AISI 316L stainless steel powder (3D Systems, Rock Hill, SC) on a ProX DMP 200 PBF machine (3D systems). The build parameters include nominal laser power of 100 W, a nominal scan velocity of 1400 mm/s, nominal hatch spacing of 50 μm. Tensile specimens were built with the tensile axis parallel to the build direction. No post-build heat treatment was applied to these samples, which were removed from the build plate *via* electrical discharge machining (EDM).

AlSi10Mg samples were manufactured from commercial purity AlSi10Mg AM powder on an EOS (Krailling, Germany) M290 SLM printer. The build parameters included a laser power of 277.5W, a scan velocity of 1300 mm/s, and the build had 5.0 mm stripe widths with 0.09 mm hatch spacing and 0.12 mm stripe section overlap. Tensile specimens were built with the tensile axis parallel to the build direction. The commonly performed stress-relief anneal thermal processing step was omitted in lieu of the electropulsing. Samples were removed from the build plate *via* wire EDM.

Electropulsing was performed using a Gleeble®® 3500 (Dynamic Systems Inc., Poestenkill, NY) thermo-physical simulator. The Gleeble® is conventionally used to replicate microstructures resulting from dynamic thermomechanical loading conditions (such as those encountered in welding or hot forming operations) that are otherwise very difficult or impossible using traditional furnace or mechanical tests. Thermocouple-instrumented samples in the Gleeble®® are heated resistively using a 100 KVA single-phase AC transformer similar to that used for resistance welding.

Thermocouples attached to the test sample interface with a closed-loop thermal control system that controls transformer output to affect the magnitude of heat generated resistively within the test sample. The Gleeble® thermal control system is able to precisely control dynamic heating rates as high as 10,000°C/sec. Additionally, force can be applied to the sample during heating/cooling via a closed-loop hydraulic servo mechanism.

The electropulse samples were held in the Gleeble®® chamber using copper (Cu) grips and the load minimized such that minimal stress was imparted on the samples during loading and unloading. The electropulsing tests were performed in force-control-mode, meaning that the displacement between the jaws was adjusted to during the tests such that zero load was maintained on the sample to help accommodate for small changes in sample length due to thermal expansion/contraction. Electropulsing was accomplished by operating the Gleeble®® open loop in which the magnitude of current applied to the sample was controlled by tailoring the phase angle of AC power delivered by the transformer via a silicon-controlled rectifier (SCR). The phase angle is the proportion of the sinusoidal AC current waveform where the transformer is switched on using the SCR thereby allowing current to flow through the sample. The Gleeble®® was programmed to deliver a current pulse with duration 16.67 ms (or one period of an AC cycle), followed by a 10 s natural cooling period (i.e. no output from the transformer with no external cooling applied). This natural cooling period was increased to 20 s for stainless steel materials to allow samples of this material to fully cool to room temperature. The power supply control incorporated a programmed loop to achieve the desired total number of pulses per test. The amount of current delivered to the specimen during each pulse was varied by changing the SCR phase angle delivered to the specimen. The tap setting on the Gleeble®® can also be adjusted to influence the voltage, therefore the tap setting was also increased during preliminary tests on stainless steel samples to in turn increase the current supplied to the specimen. All tests were conducted in an air with no protective atmosphere. Because the voltage and current delivered to the specimen are not variables directly monitored by the Gleeble®®, a Rogowsky coil with integral resistance weld process monitor (MM-112A, Amada Miyachi, Isehara City, Kanagawa, Japan) was placed around the Cu transformer output bus bar in the Gleeble®® such that the current flowing through the specimen could be monitored for each pulse. The peak current (in kiloamps, kA) was then reported for each pulse. The peak current readings and sample geometry were then used to calculate the current density through the sample for each pulse.

Specimens were tested in quasistatic, uniaxial tension at room temperature. Tensile tests were performed using displacement-control at a constant displacement rate of 0.2 mm/s using an MTS servo-hydraulic load frame. Strain measurements were performed real time using non-contact Digital Image Correlation (DIC). A commercial software, VIC-Gauge™, produced by Correlated Solutions Inc. (Columbia, SC), was used to measure strain in-situ.

After tensile testing, specimens were ground and polished for microscopy. Stainless steel specimens were etched using 60 wt.% HNO_3 and 40 wt.% distilled water at room temperature for approximately 60 seconds using 10 mA/cm^2 of current. AlSi10Mg samples were etched using Keller's reagent [44]. Optical microscopy was performed using a Zeiss Axio Observer. Electron microscopy was performed using a Zeiss Supra 55VP field emission scanning electron microscope (SEM). Electron backscatter diffraction (EBSD) was performed in this microscope using Oxford HKL AZtec™ software. EBSD data were processed using MTEX [45], an extension for MATLAB™.

1.3. Results

1.3.1. Electropulsing 316 Stainless Steel

Two stainless steel specimens were electropulsed. Both were electropulsed with the same nominal settings, which produced a maximum current in the specimens of 5 kA. This corresponds to a current density of 0.81 kA/mm^2. These specimens will be referred to as 316_Epulse01 and 316_Epulse02. 5 pulses were applied to 316_Epulse01 and 10 pulses to 316_Epulse02. Plots of controller power angle for the first and fourth pulses applied to this sample are provided in Figure 2. For all but the fourth pulse, the controller fired a single pulse, while two pulses were applied to the sample during the fourth pulse. When a single pulse was applied to the sample, the maximum sample temperature was approximately 820° C and the duration of the pulse was approximately 0.01 seconds. When two pulses were applied to the sample, the sample reached a temperature of 893° C and the pulse lasted approximately 0.02 seconds. This only occurred during electropulsing of sample 316_Epulse02.

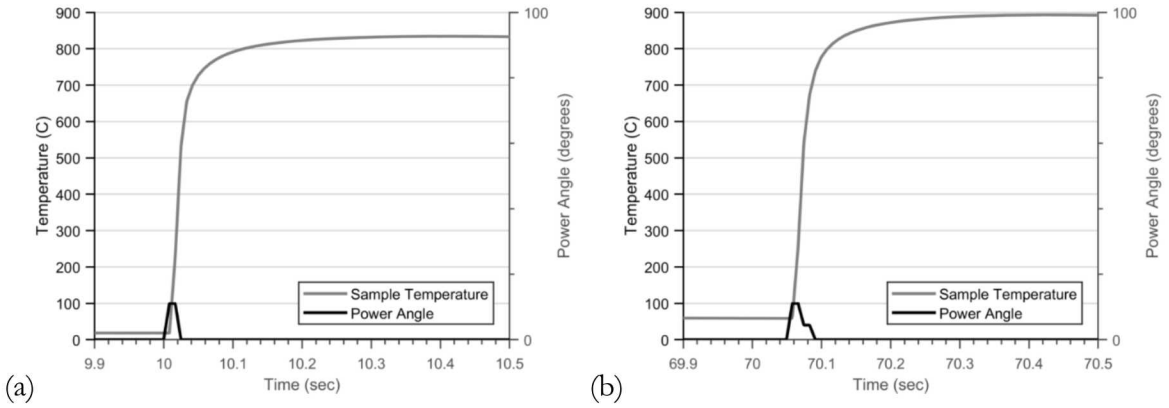

Figure 2. ***For sample 316_Epulse02, the power angle for (a) the first pulse and (b) the fourth pulse are plotted (black lines). Sample temperature for these two pulses are also plotted.***

Representative temperature *versus* time data from 316_Epulse02 are provided in Figure 3. When an electrical pulse was applied, the specimen reached its maximum temperature within approximately 0.2 seconds. Specimens remained over 800° C for approximately 1 second, then cooled to room temperature within approximately 20 seconds.

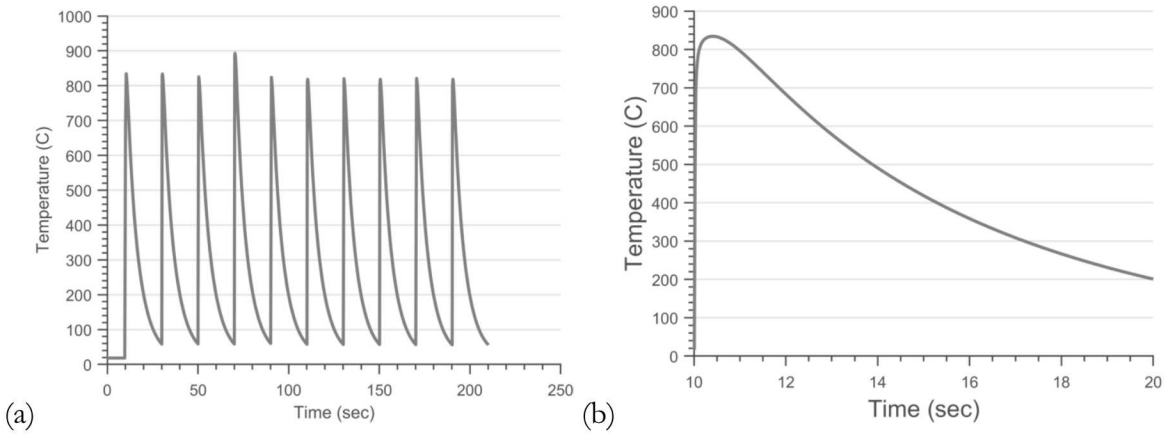

Figure 3. ***Sample temperature*** **versus** ***time is plotted for sample 316_Epulse02 for all 10 cycles applied in (a). The image in (b) highlights sample temperature*** **versus** ***time for one pulse.***

After electropulsing, each specimen was ground flat, polished, and etched using the etching procedure described in the previous section. Vickers hardness was measured in the grip and gauge regions of both specimens. Values of 230±5 were measured in the grip and gauge regions of both specimens.

Optical images revealed significant differences between the grip and gauge regions of specimen 316_Epulse02. Optical images of the gauge and grip region of this sample are shown in Figure 4. Melt pool boundaries can be observed both in the grip and gauge regions of the specimen. A few of these are labelled in Figure 4. The etching response thus suggests that microsegregation associated with the melt pool boundary did not change appreciably. In the grip portion of the sample, the etching response shows typical cellular structure associated with solidification substructure in rapidly solidified austenitic stainless steel [46]. This cellular structure is highlighted in Figure 4. In the gauge region, these cell boundaries are not visible. These images indicate that the chemical segregation in the gauge is significantly lower than that in the grip. No significant differences were observed between the grip and gauge region of a specimen that was given only 5 pulses, specimen 316_Epulse01.

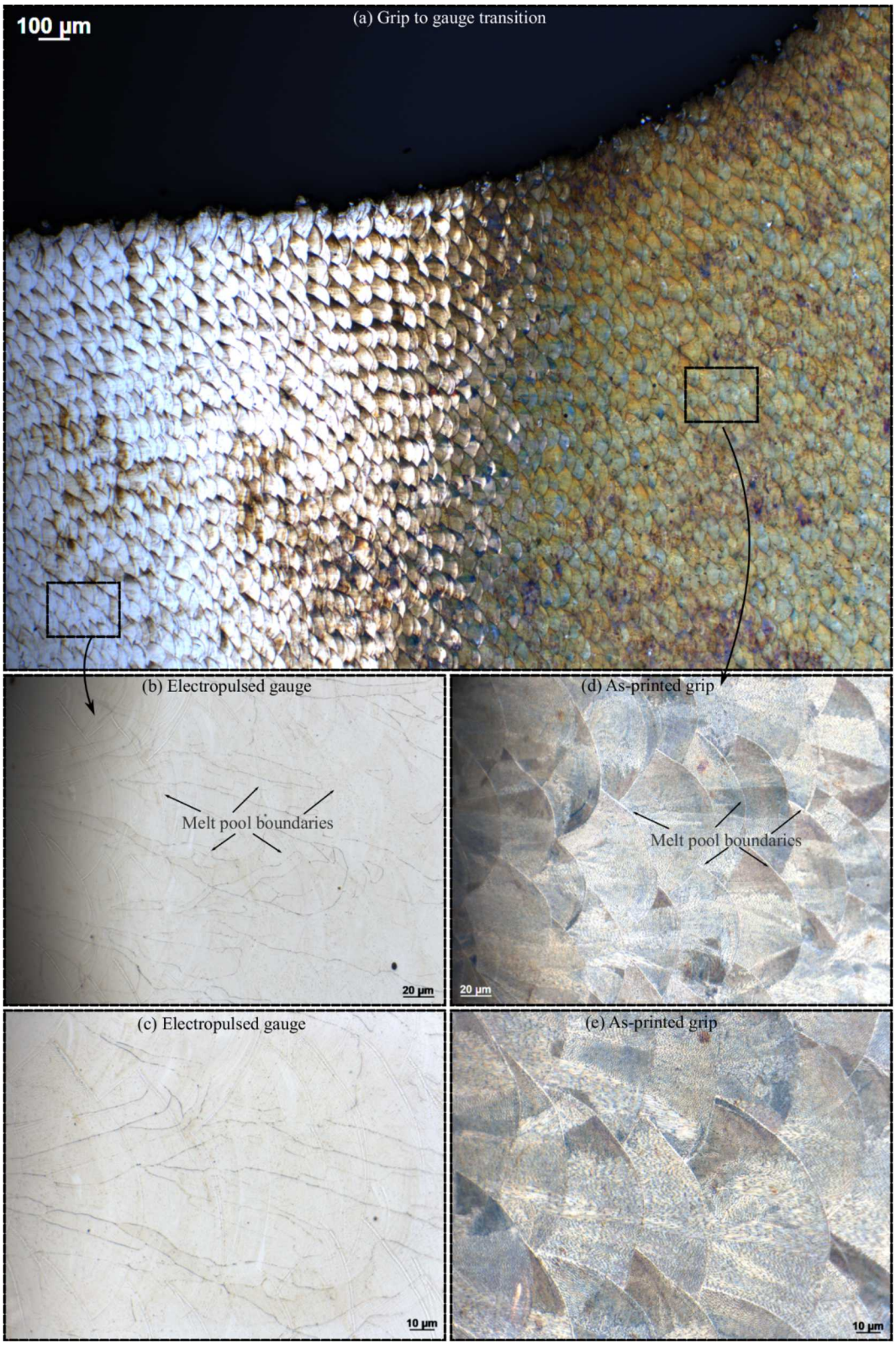

Figure 4. ***Representative optical images of a 316 SS specimen that was electropulsed 10 times with a maximum current of 5 kA are shown. Both the specimen grip and gauge, as well as the transition between the two, can be seen in (a). High-magnification images of both the grip and gauge are provided in (b) to (d).***

EBSD data were collected from the grip and gauge regions of specimen 316_Epulse02 using a 2 μm stepsize. EBSD data from the grip region are plotted as inverse pole figure (IPF) maps colored with respect to the tensile direction (TD) and short transverse direction (STD) in Figure 5. EBSD data from the gauge region are plotted as IPF maps colored with respect to the TD and STD in Figure 6. No significant difference in grain size, shape, or orientation between the grip and gauge regions can be seen in these images. To visualize the dislocation substructure created by the rapid cooling associated with SLM, EBSD data from the grip and gauge regions are plotted as kernel average misorientation (KAM) maps in Figure 7. Recall from reference [47] that KAM is one of several methods to visualize the lattice curvature created by geometrically necessary dislocations. While not a quantitative measurement of dislocation density, KAM maps allow qualitative differences in the density of geometrically necessary dislocations to be evaluated. The KAM maps in Figure 7(a) and (b) suggest that there are no significant differences in the density of geometrically necessary dislocations between the grip and gauge regions of this specimen. It is important to note that the chemical microsegregation visible in the optical images shown in Figure 4 are not visible in these EBSD data and are too fine to be detected using EDS [6, 48].

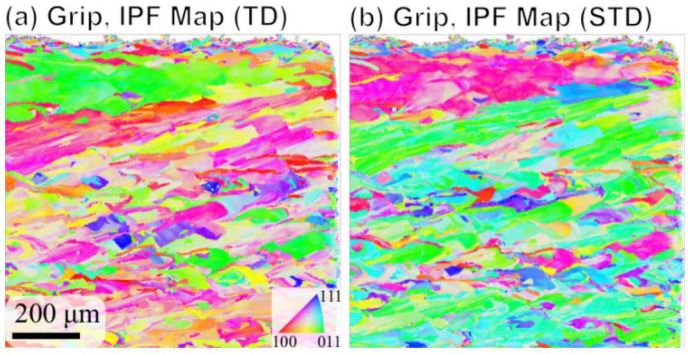

Figure 5. ***EBSD data from the grip region of a 316 SS specimen that was electropulsed 10 times with a maximum current of 5 kA are plotted as IPF maps colored with respect to the (a) tensile direction (TD) and (b) short transverse direction (STD). Optical images in Figure 4 show that the microstructure in the grip region of this specimen was not significantly altered by electropulsing.***

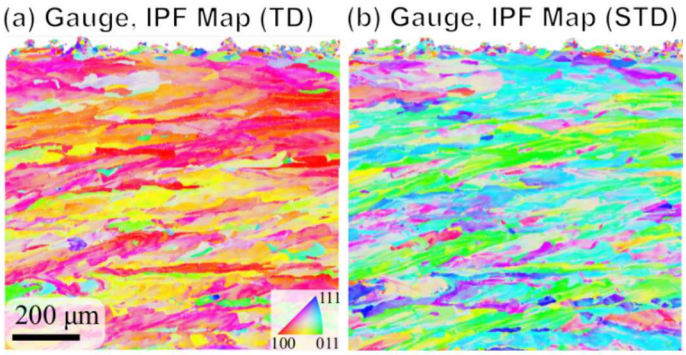

Figure 6. ***EBSD data from the gauge region of a 316 SS specimen that was electropulsed 10 times with a maximum current of 5 kA are plotted as IPF maps colored with respect to the (a) tensile direction (TD) and (b) short transverse direction (STD). Optical images in Figure 4 show that electropulsing altered chemical microsegregation in the gauge region of this sample.***

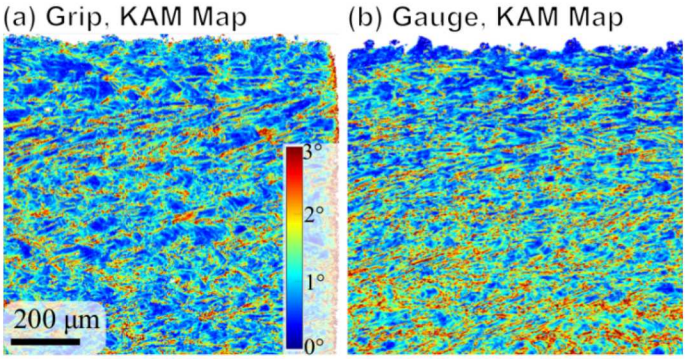

Figure 7. ***EBSD data from the (a) grip and (b) gauge regions of a 316 SS specimen that was electropulsed 10 times with a maximum current of 5 kA are plotted as kernel average misorientation (KAM) maps.***

1.3.2. Electropulsing Aluminum Magnesium Silicon

A total of six AlSi10Mg samples were electropulsed for this study. The specimens and conditions under which each specimen was treated are listed in Table 1-2. Each AlSi10Mg specimen that was electropulsed is labelled as AlEpulse-0X, where "0X" is a unique identifier for each specimen. Specimens were numbered in order of increasing average peak current density applied to the specimen. For comparison, two additional AlSi10Mg specimens from the same build plate were characterized for this study. One specimen was in the as-received (as-printed) condition while a second specimen was annealed in air at 300° C for two hours. These specimens will be referred to as the "as-received" and "heat-treated" samples, respectively.

Table 1-2. A test matrix listing the conditions applied to each of the AlSi10Mg used in this study is provided. One specimen was tested in the as-received (as-built) condition, and a second was annealed in air for 2 hours at 300° C. The six other samples were all electropulsed. For each of these samples, the average peak current density, average peak sample temperature, and number of pulses applied are listed.

Specimen	Average Peak Current Density (kA/mm^2)	Average Peak Sample Temperature (°C)	Number of Pulses Applied
As-received	-	-	-
Heat-treated (300° C, 2 hours)	-	-	-
AlEpulse-01	1.32	196	100
AlEpulse-02	1.40	245	20
AlEpulse-03	1.53	290	20
AlEpulse-04	1.68	365	100
AlEpulse-05	1.78	377	20
AlEpulse-06	1.98	430	15

As was observed when electropulsing stainless steel samples, the controller occasionally applied two electrical pulses to AlSi10Mg samples rather than one. For example, plots of controller power angle for the first and second pulses applied to sample AlEpulse-03 are provided in Figure 8. In the AlSi10Mg samples, a double pulse typically increased sample temperature by more than 100° C, as shown in this figure. The occurrence of these double pulses appeared to be random, occurring approximately once every 15 pulses. To avoid confusion, the average peak sample temperature reported in Table 1-2 is only for pulses during which a single electrical pulse was sent to the sample. Samples AlEpulse-05 and AlEpulse-06 did not receive any "double-pulse" cycles during electropulsing. As for the stainless steel samples, a single pulse lasted approximately 0.01 seconds and a double pulse lasted approximately 0.02 seconds.

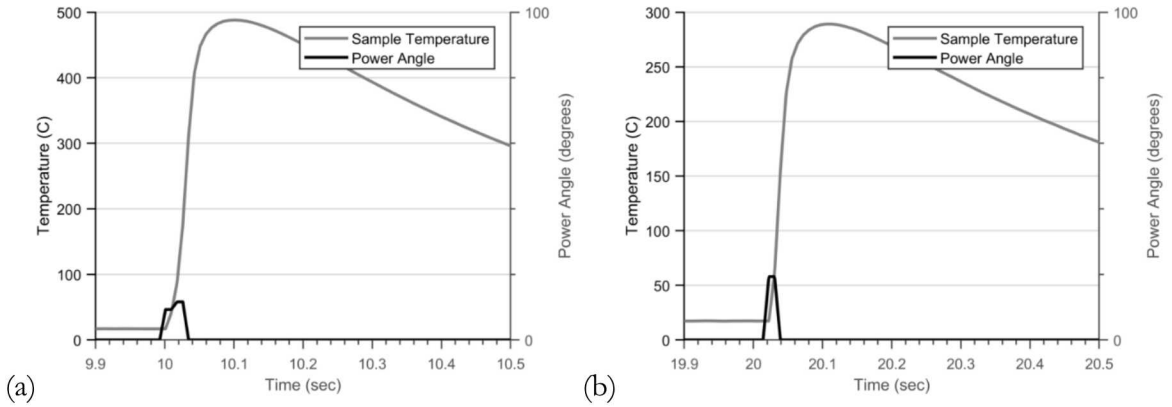

Figure 8. ***For sample AlEpluse-03, the power angle for (a) the first pulse and (b) the second pulse are plotted (black lines). Sample temperature for these two pulses are also plotted.***

Representative temperature *versus* time data for the first five electropulses applied to sample AlEpulse_03 are provided in Figure 9. As Table 1-2 summarizes, the average peak sample temperature varied significantly with the applied current density. Regardless of the maximum

temperature reached by the sample during pulsing, though, the specimen reached its maximum temperature within approximately 0.2 seconds of applying an electrical pulse. This can be seen in the plot provided in Figure 9(b). Regardless of the maximum specimen temperature, the specimen temperature dropped below 100° C within 1 second of reaching the maximum temperature. Specimens returned to room temperature within approximately 2 seconds of applying an electrical pulse.

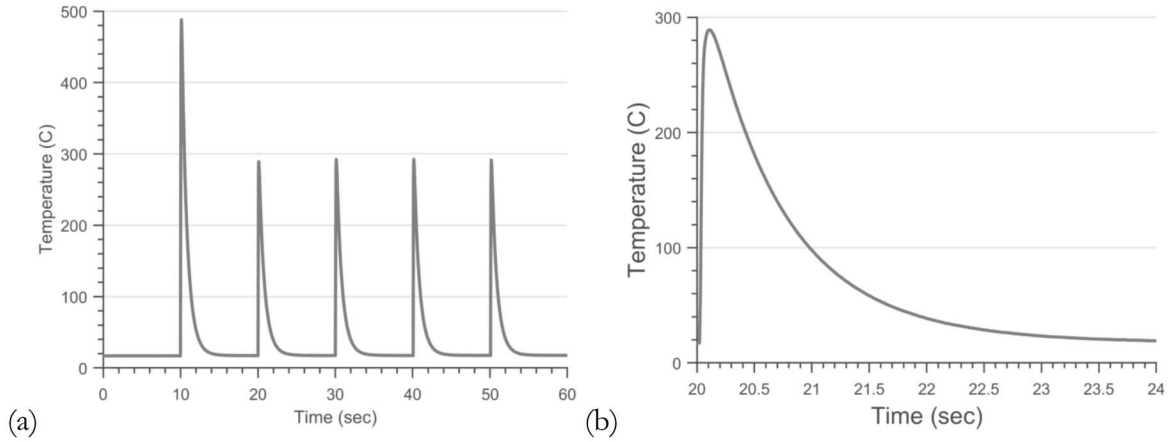

Figure 9. ***For sample AlEpluse-03, sample temperature*** **versus** ***time is reported for (a) the first five pulses applied to the sample and (b) for the two seconds after the second electrical pulse was applied to this sample.***

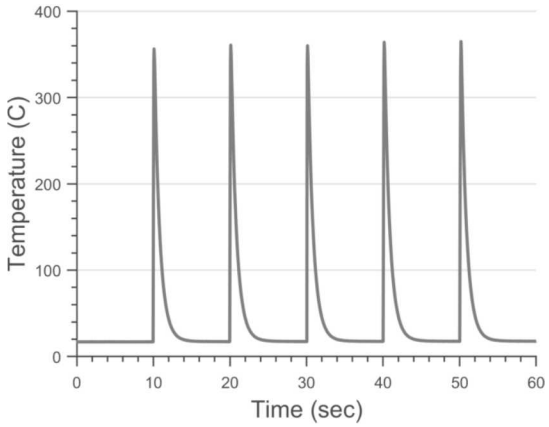

Figure 10. ***For sample AlEpluse-04, sample temperature*** **versus** ***time is reported for the first five pulses applied to the sample.***

After treatment, the as-received, heat-treated, and five of the six electropulsed samples were elongated to failure in tension. Specimen AlEpulse-06 was not tested in tension. The yield and ultimate strengths and the ductility of these specimens are listed in Table 1-3. Tensile data from four of these specimens are plotted in Figure 11.

Table 1-3. The mechanical properties (yield stress, ultimate stress, and ductility) for the 8 AlSi10Mg samples used in this study are listed.

Specimen	Yield Stress (MPa)	Ultimate Stress (MPa)	Ductility (% Elongation)
As-received	215	350	2.12
Heat-treated (300° C, 2 hours)	115	232	13.76
AlEpulse-01, 1.32 kA/mm^2 X100	167	341	3.26
AlEpulse-02, 1.40 kA/mm^2 X20	180	338	2.33
AlEpulse-03, 1.53 kA/mm^2 X20	173	316	2.6
AlEpulse-04, 1.68 kA/mm^2 X100	117	285	6.09
AlEpulse-05, 1.78 kA/mm^2 X20	163	304	4.68

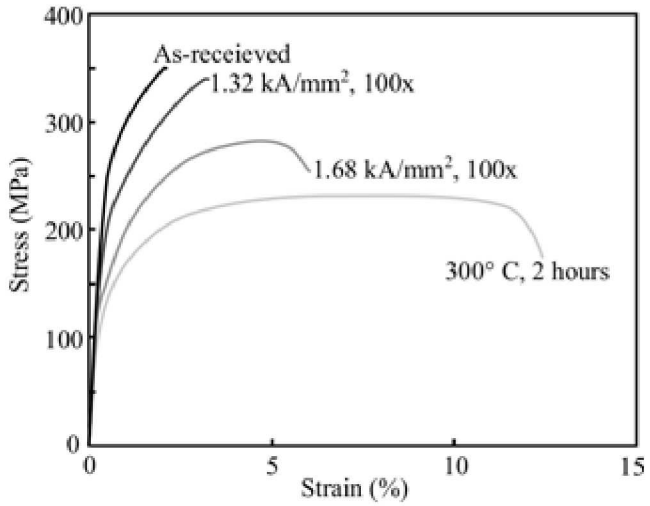

Figure 11. ***Plots of engineering stress* versus *engineering strain for four AlSi10Mg samples are provided.***

To clearly observe the effects of electropulsing on the Si distribution within an AlSi10Mg sample, specimen AlEpulse-06 was ground, polished, and etched. It was not mechanically deformed after electropulsing. An optical image of this specimen is provided in Figure 13. This image suggests that the distribution of Si in the gauge (electropulsed) region of specimen AlEpulse-06 was significantly different than that in the grip (untreated) region of this specimen. To observe differences in Si distribution between the gauge and grip regions of this specimen, electron channeling contrast (ECCI) images of both regions were taken and are shown in Figure 13. Si appears as white in these images; some of the Si-rich regions are labelled in Figure 13. These images indicate that electropulsing only affected the microstructure within the gauge region of this specimen.

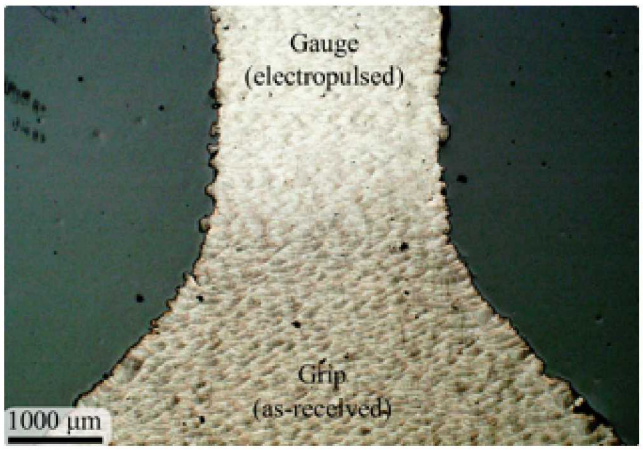

Figure 12. ***An optical image of specimen AlEpulse-06 after electropulsing is provided. This sample was polished and etched.***

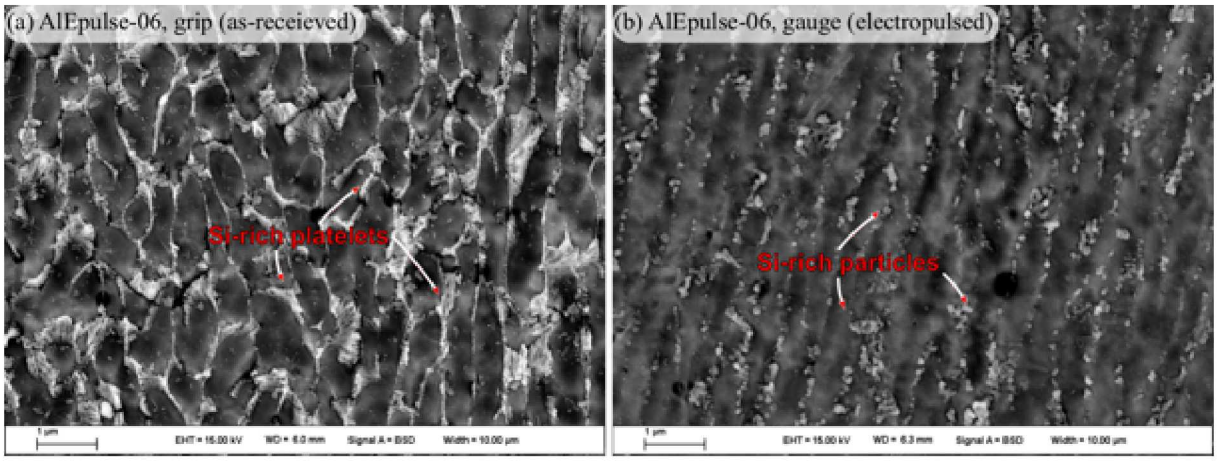

Figure 13. ***Electron channeling contrast images of sample AlEpulse-06 after etching is provided. A low-magnification image of this specimen is shown in Figure 12. (a) shows the grip region and (b) shows the gauge. Clear differences in the morphology of the Si-rich phase can be seen.***

All seven of the specimens that were elongated to failure were also ground and polished after mechanical deformation. These specimens were not etched. ECCI images were taken within the gauge regions of all seven of these samples; care was taken to perform imaging away from the most-deformed region of the specimen near the fracture surface. ECCI images of **X** of the specimens are provided in Figure 14.

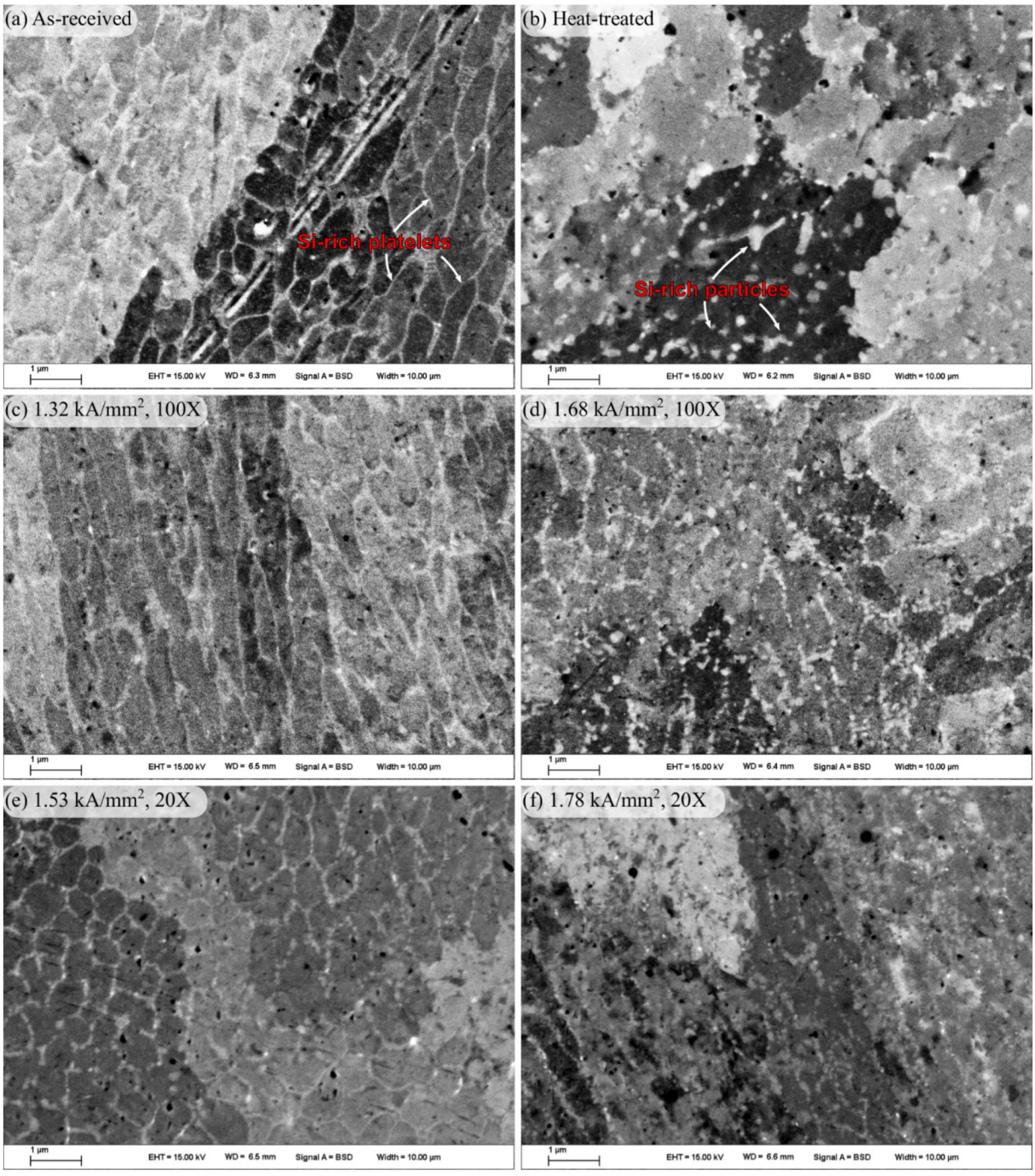

Figure 14. ***Electron channeling contrast images of polished AlSi10Mg samples are provided. The samples in (a) and (b) were in the as-received and heat-treated conditions, respectively. Samples in (c) to (f) were electropulsed. The average peak current density and number of pulses applied to each sample are listed. Si-rich platelets and/or particles appear as white in images of all specimens. All images are at the same scale.***

After imaging, Vickers hardness values were measured within the deformed gauge region of all seven of these samples. For each specimen, care was taken to perform hardness measurements away from the most-deformed region of the gauge region near the fracture surface. Vickers hardness was also

measured in the undeformed gauge region of specimen AlSi10Mg. All Vickers hardness values are reported in Table 1-4.

Table 1-4. Vickers hardness values for the 8 AlSi10Mg samples used in this study are listed.

Specimen	Average Vickers Hardness (HV)
As-received	127
Heat-treated (300° C, 2 hours)	77
AlEpulse-01, 1.32 kA/mm^2 X100	117
AlEpulse-02, 1.40 kA/mm^2 X20	131
AlEpulse-03, 1.53 kA/mm^2 X20	121
AlEpulse-04, 1.68 kA/mm^2 X100	97
AlEpulse-05, 1.78 kA/mm^2 X20	109
AlEpulse-06, 1.98 kA/mm^2 X15	101

To characterize how electropulsing altered the Si in SLM AlSi10Mg samples, EDS was performed on an as-received sample and two electropulsed samples, samples AlEpulse-01 and AlEpulse-04. EDS was also performed on the heat-treated samples. For all conditions, it was observed that Al and Mg were homogeneously distributed throughout the microstructure. Representative EDS data from the as-received specimen showing the distribution of Al, Si and Mg are plotted in Figure 15. The distribution of Si in the as-built material as a cellular structure is apparent. It is important to note that the cell spacing of Si in this sample is near the spatial resolution of EDS. EDS data indicated that the distribution of Si varied depending on the treatment conditions. EDS data showing the distribution of Si in the as-received, heat-treated, AlEpulse-01, and AlEpulse04 samples are plotted in Figure 16.

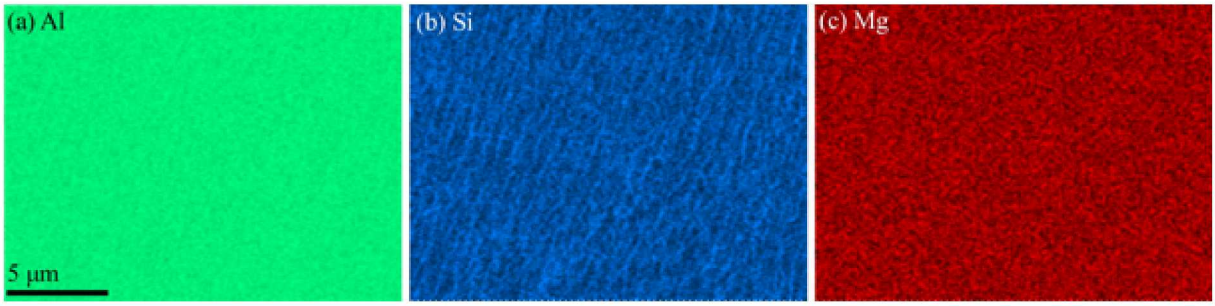

Figure 15. ***Representative EDS data from an as-received AlSi10Mg sample are provided.***

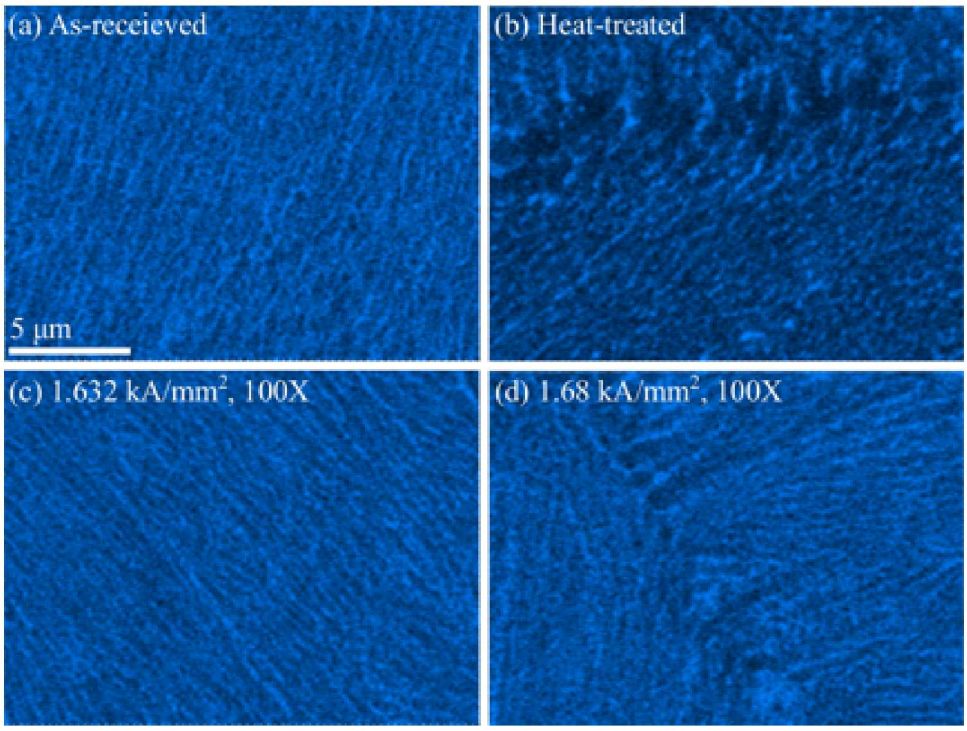

Figure 16. ***EDS data highlighting the distribution of Si in (a) as-received, (b) heat-treated, and (c) and (d) electropulsed AlSi10Mg samples are shown.***

To characterize how electropulsing altered the grain and dislocation structures of SLM AlSi10Mg samples, EBSD data were collected from the as-received grip and electropulsed gauge regions of sample AlEpulse-06 using a stepsize of 0.4 μm. Recall from Table 1-2 that this sample was pulsed 20 times with an average peak current density of 1.98 kA/mm^2. Representative EBSD data from one of the datasets collected from the grip region are plotted as IPF maps colored with respect to the TD and STD, a band contrast map, and a KAM map in Figure 17. Representative EBSD data from one of the datasets collected from the gauge region are plotted as IPF maps colored with respect to the TD and STD, a band contrast map, and a KAM map in Figure 18. While not quantitative measurements of dislocation density, the band contrast and KAM maps suggest that the dislocation density in the gauge region of this specimen is less than that in the grip region.

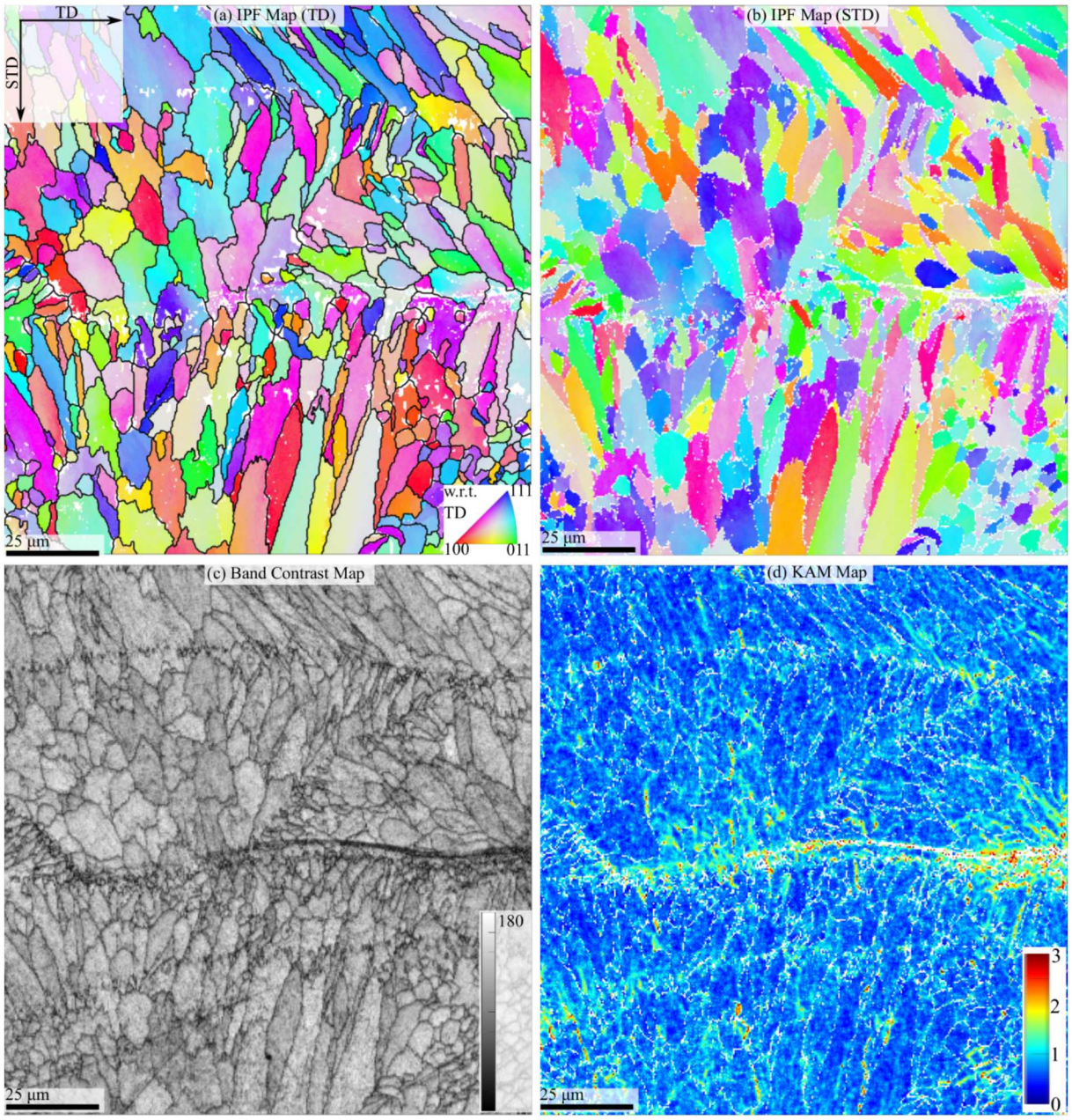

Figure 17. ***EBSD data from the as-received grip region of specimen AlEpulse-06 are plotted as an IPF maps colored with respect to the (a) TD and (b) STD, (c) an image quality (band contrast) map, and a (d) KAM map. Black lines overlaid on the map in (a) highlight high-angle (>5°) grain boundaries.***

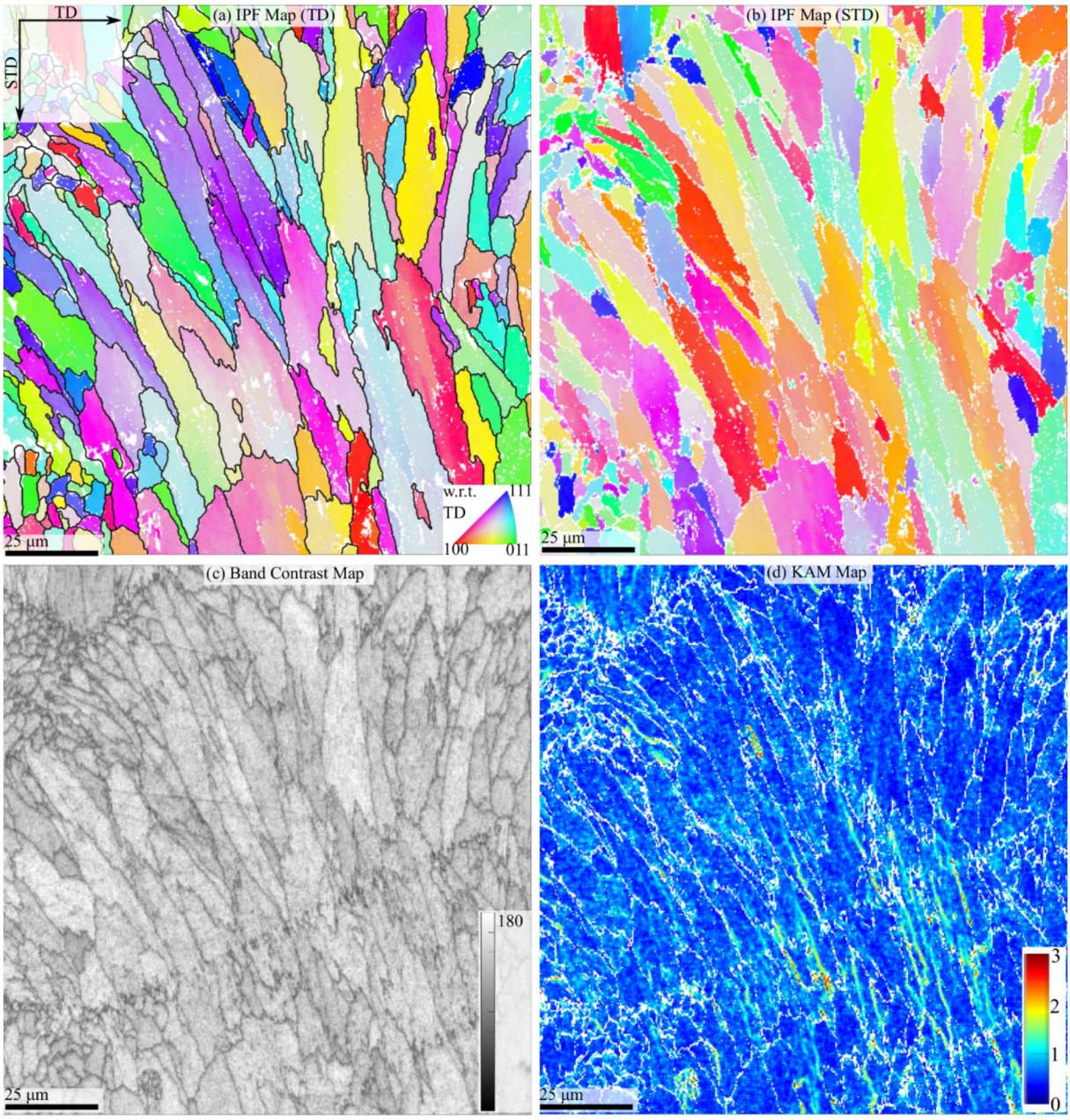

Figure 18. ***EBSD data from the electropulsed gauge region of specimen AlEpulse-06 are plotted as an IPF maps colored with respect to the (a) TD and (b) STD, (c) an image quality (band contrast) map, and a (d) KAM map. Black lines overlaid on the map in (a) highlight high-angle (>5°) grain boundaries.***

1.4. Discussion

The present study examined if electropulsing could be used to perform microstructural modification on additively manufactured stainless steel (316L) and aluminum alloys (AlSi10Mg). Recent studies have demonstrated that, compared to conventional wrought materials, additively manufactured metals can require significantly higher temperatures and longer exposure times to produce similar microstructural modifications. It was thus unclear if electropulsing would affect additively

manufactured materials in the same way as the wrought, cast, or rolled materials examined in previous studies of electropulsing. The observations presented in the previous section and the implications of these observations are now discussed in more detail.

1.4.1. Microstructural modification of 316L SS

Figure 4 demonstrates that electropulsing significantly reduced the microsegregation associated with SLM of stainless steels. The EBSD data presented in Figure 5, Figure 6, and Figure 7 indicate that this was accomplished without significantly altering the dislocation substructure or grain structure created by the rapid cooling associated with SLM. Moreover, no significant difference Vickers hardness was measured between the grip and gauge regions of this specimen. This suggests that electropulsing can be used to remove microsegregation in SLM 316L SS materials without significantly altering other microstructural features. Detailed analysis using transmission electron microscopy would be necessary to fully assess the chemical homogenization in this material after electropulsing [6, 48].

Susan *et al.* [7] demonstrated that microsegregation in SLM 316L SS could largely be eliminated by annealing this material for 2 hours at 800° C. They noted, though, that this heat treatment reduced the Rockwell B hardness of this material from 94 to 90, which corresponds approximately to a reduction in Vickers hardness from 209 to 183. It is likely that annealing for 2 hours at 800° C allowed at least partial recovery of the dislocation substructure created during SLM. In contrast, EBSD and hardness measurements suggest that electropulsing can remove microsegregation in SLM 316L SS without significantly altering the dislocation structure. In their study of the mechanical properties of stainless steels fabricated using LENS, Smith *et al.* [48] concluded that "*the mechanical properties of deposited austenitic stainless steels can be influenced by controlling thermomechanical history during the manufacturing process to alter the character of compositional microsegregation and the amount of induced plastic deformation.*" The present study suggests that electropulsing may provide a tunable method to modify microsegregation in AM stainless steels without affecting dislocations and may thus provide a more controlled method of fine-tuning mechanical properties.

It is also important to note that electropulsing provides a significantly more rapid method for altering microsegregation in AM stainless steels. The study of Susan *et al.* [7] suggests that annealing for approximately 2 hours at 800° C is necessary to remove microsegregation in SLM 316L SS. In the present study, electropulsing appears to have removed, or at least significantly reduced, microsegregation after the application of only 10 electrical pulses. Each pulse lasts 0.01 seconds, though approximately 20 seconds after pulsing are required for the specimen to cool to room temperature. Even conservatively, this study suggests that, using electropulsing, only 200 seconds are needed to produce a similar level of homogenization in SLM 316L SS to that observed by Susan *et al.* [7] after 2 hours at 800° C. In essence, electropulsing was at least thirty-six times faster at altering the microstructure of SLM 316L SS than conventional thermal annealing.

1.4.2. Microstructural modification of AlSi10Mg

As Figure 13(a), Figure 14(a), and Figure 15 show, in the as-built AlSi10Mg material used in this study, the α-Al + silicon terminal interdendritic eutectic constituent was disturbed as a cellular structure. The spacing of cells was approximately 1 μm. As Figure 14(b) and Figure 16(b) show, annealing this material for two hours at 300° C created spheroidized Si distributed throughout the α-Al phase. This significantly decreased the yield strength, UTS, and Vickers hardness of the AlSi10Mg material.

Figure 12, Figure 13, Figure 14, and Figure 16 demonstrate that, for some combinations of current density and number of pulses, electropulsing significantly altered the distribution of the cellular, Si-rich, interdendritic constituent. In particular, the microstructures of samples AlEpulse-04 and AlEpulse-06 clearly contained partially spheroidized Si. ECCI images and EDS data suggest that, qualitatively, compared to the microstructure of the heat-treated sample, the Si-rich, terminal eutectic constituent was not as spheroidized in these electropulsed samples as in the heat-treated sample. Figure 12, Figure 13, Figure 14, and Figure 16 also show that relatively little spheroidization occurred in other electropulsed samples, such as AlEpulse-01. The EBSD data provided in Figures 17 and 18 suggest that electropulsing may have allowed some of the residual dislocation structure in the AlSi10Mg material to recover, though more work would be necessary to confirm this. EBSD data also indicate that grain size, shape, and orientation were not significantly affected by electropulsing.

As expected, the partial spheroidization of the Si-rich constituent produced by electropulsing resulted in increased part ductility and decreased part strength. This can be seen in Figure 11 and Table 1-3 and Table 1-4. No combination of current density and number of pulses examined in this study produced samples with elongation values similar to those after two hours of annealing at 300° C. However, similar mechanical properties to those observed by references [42] and [43] after the T6 heat treatment or by reference [5] after 0.25 hours of annealing at 307° C were observed following some electropulsing treatments, notably those given to samples AlEpulse-04 and AlEpulse-06.

As for the SLM 316L SS material, it appears that electropulsing may provide a much more rapid path to modifying the microstructure and mechanical properties of SLM AlSi10Mg materials than conventional thermal annealing approaches. The microhardness values of sample AlEpulse-06, which was pulsed 15 times at a current density of 1.98 kA/mm^2, are comparable to those reported by reference [5] after 0.25 hours of annealing at 307° C. For the AlSi10Mg material used in this study, Figure 9 and Figure 10 show that the material cooled from its peak temperature to 100° C within ≈1 second and reached room temperature within ≈2 seconds. While not performed for this study, these results suggest that comparable mechanical properties to those observed after annealing at 307° C for 0.25 hours can be produced by ≈30 seconds of electropulsing at a current density of ≈2 kA/mm^2. Further study will be necessary to determine if larger current densities or increased number of pulses can attain ductilities of ≈15%.

1.4.3. The effects of current density on microstructural modification

Perhaps the most surprising finding of this study was the extent to which microstructural modifications produced by electropulsing depended on the number of pulses applied and the current density. For SLM 316L SS, optical images suggested that 5 pulses did not significantly affect microsegregation; however, 10 pulses appears to significantly reduce microsegregation compared to the as-built 316L SS. For the AlSi10Mg material, it was observed that microstructural changes produced by electropulsing were highly sensitive to the current density applied to the sample. As Table 1-3 summarizes, a 15% increase in current density from 1.53 to 1.78 kA/mm^2 nearly doubled the ductility of the material. Conversely, an increase from 1.40 to 1.53 kA/mm^2 did not significantly alter the ductility of the material. In addition, as Figure 4 and Figure 12 show, microstructural changes from electropulsing were restricted to the gauge region of the specimen where the current density was the largest.

Two important conclusions can be drawn from these results. First, microstructural changes due to electropulsing appear to be restricted to areas of the microstructure where the resistance is lowest. In

the present study, this corresponds to the thinnest areas of the specimen. Second, to obtain a desired microstructure using electropulsing, both current density and number of pulses applied to the sample can be varied to reach a desired microstructure. However, lacking a mechanistic understanding of electropulsing it is unclear *a priori* what combination of current density and number of pulses should be selected to obtain a desired microstructure. It is hoped that this study motivates future investigation of the mechanisms of electropulsing so that this technique can be applied to future postprocessing needs.

1.5. Conclusions

The present study demonstrated that electropulsing can be used to rapidly modify the microstructures of two representative SLM materials: 316L SS and AlSi10Mg. In particular, we observed that:

1. electropulsing reduced microsegregation in 316L SS without significantly altering the dislocation and grain structures created by the SLM processes, and
2. electropulsing partially spheroidized the cellular, Si-rich, eutectic constituent created by rapid solidification during SLM. This increased the ductility and decreased the strength of electropulsed AlSi10Mg samples.

For both materials, these microstructural modifications were produced at least an order of magnitude faster *via* electropulsing than *via* conventional thermal annealing. It was also observed that the microstructural changes by electropulsing were highly sensitive to the applied current density and the number of electrical pulses. These results indicate that electropulsing may provide a much more rapid and controllable method for modifying the microstructures of SLM materials than conventional annealing approaches. Indeed, it may be possible to specifically tune the properties of an entire structure by careful part design and subsequent electropulsing. It is also clear that an understanding of the mechanisms of electropulsing is critically needed in order to properly use this technique to control the microstructure of SLM materials.

This page left blank

REFERENCES

i. 1. Jason R Trelewicz, Gary P Halada, Olivia K Donaldson and Guha Manogharan, *Jom* 2016, vol. 68, pp. 850-859.

ii. 2. Naoki Takata, Hirohisa Kodaira, Keito Sekizawa, Asuka Suzuki and Makoto Kobashi, *Materials Science and Engineering: A* 2017, vol. 704, pp. 218-228.

iii. 3. Naor Elad Uzan, Roni Shneck, Ori Yeheskel and Nachum Frage, *Materials Science and Engineering: A* 2017, vol. 704, pp. 229-237.

iv. 4. Christopher B Finfrock, Andrea Exil, Jay D Carroll and Lisa Deibler, *Metallography, Microstructure, and Analysis* 2018, vol. 7, pp. 443-456.

v. 5. Pin Yang, Mark A Rodriguez, Lisa A Deibler, Bradley H Jared, James Griego, Alice Kilgo, Amy Allen and Daniel K Stefan, *Journal of Materials Research* 2018, vol. 33, pp. 1701-1712.

vi. 6. Thale R Smith, Joshua D Sugar, Julie M Schoenung and Chris San Marchi, *Jom* 2018, vol. 70, pp. 358-363.

vii. 7. Don Susan, Dan Kammler, Mark Rodriguez, Joseph Michael, Zahra Ghanbari, Bradley Jared and Christina Profazi, In *Solid Freeform Fabrication*, (2018).

viii. 8. Hans Conrad, *Materials Science and Engineering: A* 2000, vol. 287, pp. 227-237.

ix. 9. OA Troitskii, *Strength of Materials* 1976, vol. 8, pp. 1466-1471.

x. 10. OA Troitskii, *ZhETF Pisma Redaktsiiu* 1969, vol. 10, p. 18.

xi. 11. SH Xiao, JD Guo, SD Wu, GH He and SX Li, *Scripta materialia* 2002, vol. 46, pp. 1-6.

xii. 12. Guoliang Hu, Guoyi Tang, Yaohua Zhu and Chanhung Shek, *Metallurgical and Materials Transactions A* 2011, vol. 42, p. 3484.

xiii. 13. RS Qin, Edwin I Samuel and Arghya Bhowmik, *Journal of materials science* 2011, vol. 46, pp. 2838-2842.

xiv. 14. Xiaofeng Xu, Yuguang Zhao, Bingdong Ma, Jiatao Zhang and Ming Zhang, *Materials Science and Engineering: A* 2014, vol. 612, pp. 223-226.

xv. 15. S To, Zhu YH, Lee WB, Tang GY and Liu XM, *Materials transactions* 2009, vol. 50, pp. 1105-1112.

xvi. 16. Hui Song and Zhong-Jin Wang, *Materials Science and Engineering: A* 2008, vol. 490, pp. 1-6.

xvii. 17. Yanbin Jiang, Guoyi Tang, Chanhung Shek and Wei Liu, *Journal of Alloys and Compounds* 2011, vol. 509, pp. 4308-4313.

xviii. 18. Ting Hao, Hisanori Tanimoto and Hiroshi Mizubayashi, *Materials transactions* 2005, vol. 46, pp. 2898-2907.

xix. 19. R Takemoto and H Mizubayashi, *Acta metallurgica et materialia* 1995, vol. 43, pp. 1495-1504.

xx. 20. Yizhou Zhou, Jingdong Guo, Wei Zhang and Guanhu He, *Journal of materials research* 2002, vol. 17, pp. 3012-3014.

xxi. 21. S To, Zhu YH, Lee WB and Liu XM, *Materials transactions* 2010, pp. 1010041185-1010041185.

xxii. 22. Zhou Yizhou, Zeng You, He Guanhu and Zhou Benlian, *Journal of Materials Research* 2001, vol. 16, pp. 17-19.

xxiii. 23. XL Wang, JD Guo, YM Wang, XY Wu and BQ Wang, *Applied physics letters* 2006, vol. 89, p. 061910.

xxiv. 24. A Rahnama and RS Qin, *Scripta Materialia* 2015, vol. 96, pp. 17-20.

xxv. 25. Yizhou Zhou, Wei Zhang, Manling Sui, Douxing Li, Guanhu He and Jingdong Guo, *Journal of materials research* 2002, vol. 17, pp. 921-924.

xxvi. 26. WJ Lu, XF Zhang and RS Qin, *Materials Science and Technology* 2015, vol. 31, pp. 1530-1535.
xxvii. 27. Ju-Won Park, Hye-Jin Jeong, Sung-Woo Jin, Moon-Jo Kim, Kyooyoung Lee, Jae Joong Kim, Sung-Tae Hong and Heung Nam Han, *Materials Characterization* 2017, vol. 133, pp. 70-76.
xxviii. 28. Ke Huang, Cyril Cayron and Roland E Logé, *Materials Characterization* 2017, vol. 129, pp. 121-126.
xxix. 29. Hans Conrad, Nasser Karam and Sardari Mannan, *Scripta metallurgica* 1983, vol. 17, pp. 411-416.
xxx. 30. Richard S Sorbello, *Physical Review B* 1985, vol. 31, p. 798.
xxxi. 31. James R Black, *IEEE Transactions on Electron Devices* 1969, vol. 16, pp. 338-347.
xxxii. 32. Qing Xu, Lei Guan, Yanbin Jiang, Guoyi Tang and Shaonan Wang, *Materials letters* 2010, vol. 64, pp. 1085-1087.
xxxiii. 33. Duo Zhang, Suet To, Yao Hua Zhu, Hao Wang and Guo Yi Tang, *Metallurgical and Materials Transactions A* 2012, vol. 43, pp. 1341-1346.
xxxiv. 34. GQ Teng, YS Chao, ZH Lai and L Dong, *Journal of materials science letters* 1995, vol. 14, pp. 144-145.
xxxv. 35. John C Lippold and Damian J Kotecki, *Welding Metallurgy and Weldability of Stainless Steels, by John C. Lippold, Damian J. Kotecki, pp. 376. ISBN 0-471-47379-0. Wiley-VCH, March 2005.* 2005, p. 376.
xxxvi. 36. JW Elmer, SM Allen and TW Eagar, *Metallurgical transactions A* 1989, vol. 20, pp. 2117-2131.
xxxvii. 37. Maria L Montero-Sistiaga, Miguel Godino-Martinez, Kurt Boschmans, Jean-Pierre Kruth, Jan Van Humbeeck and Kim Vanmeensel, *Additive Manufacturing* 2018, vol. 23, pp. 402-410.
xxxviii. 38. Evren Yasa and Jean-Pierre Kruth, *Procedia Engineering* 2011, vol. 19, pp. 389-395.
xxxix. 39. Yuan Zhong, Leifeng Liu, Stefan Wikman, Daqing Cui and Zhijian Shen, *Journal of Nuclear Materials* 2016, vol. 470, pp. 170-178.
xl. 40. JA Brooks, JC Williams and AW Thompson, *Metallurgical Transactions A* 1983, vol. 14, pp. 23-31.
xli. 41. Noriko Read, Wei Wang, Khamis Essa and Moataz M Attallah, *Materials & Design (1980-2015)* 2015, vol. 65, pp. 417-424.
xlii. 42. Nesma T Aboulkhair, Ian Maskery, Chris Tuck, Ian Ashcroft and Nicola M Everitt, *Materials Science and Engineering: A* 2016, vol. 667, pp. 139-146.
xliii. 43. U Tradowsky, J White, RM Ward, N Read, W Reimers and MM Attallah, *Materials & Design* 2016, vol. 105, pp. 212-222.
xliv. 44. George F Vander Voort: *Metallography, principles and practice.* (ASM International, 1999).
xlv. 45. F. Bachmann, Ralf Hielscher and Helmut Schaeben, In *Solid State Phenomena*, (2010), pp 63-68.
xlvi. 46. Stéphane Gorsse, Christopher Hutchinson, Mohamed Gouné and Rajarshi Banerjee, *Science and Technology of advanced MaTerialS* 2017, vol. 18, pp. 584-610.
xlvii. 47. Stuart I Wright, Matthew M Nowell and David P Field, *Microscopy and microanalysis* 2011, vol. 17, pp. 316-329.
xlviii. 48. Thale R Smith, Joshua D Sugar, Chris San Marchi and Julie M Schoenung, *Acta Materialia* 2019, vol. 164, pp. 728-740.

This page left blank

DISTRIBUTION

Email—Internal

Name	Org.	Sandia Email Address
Technical Library	01177	libref@sandia.gov

This page left blank

This page left blank

Sandia National Laboratories

Sandia National Laboratories is a multimission laboratory managed and operated by National Technology & Engineering Solutions of Sandia LLC, a wholly owned subsidiary of Honeywell International Inc. for the U.S. Department of Energy's National Nuclear Security Administration under contract DE-NA0003525.